

## Effect of Laser Energy on the Structure of Ni46–Ti50–Cu4 Shape-Memory Alloy

Abeer R. Abbas<sup>1\*</sup>, Kadhim A. Hebeatir<sup>1</sup> and Kadhim K. Resan<sup>2</sup>

<sup>1</sup>University of Technology, Laser and Optoelectronic Engineering dept., Baghdad, Iraq.

<sup>2</sup>AL-Mustansiriya University, College of Engineering, Baghdad, Iraq.

Received 28 October 2017; Revised 11 December 2017; Accepted 25 April 2018

### ABSTRACT

*The structural and physical properties of nickel–titanium–copper shape-memory alloy and the effect of laser irradiation on the alloy were investigated in this study. The alloy was prepared using the powder metallurgy method. Powders of 50% Ti, 46% Ni, and 4% Cu by weight were mixed and then cold-compacted at 600, 700, and 800 MPa to form cylindrical samples 11mm in diameter and 16.5 mm in length. The samples exhibited sufficient green strength for handling after compaction and were subsequently sintered at 850°C, 900°C, and 950°C for five hours in an electric vacuum tube furnace. The optimum compacting pressure and sintering temperature were identified using Minitab software. Samples prepared under the optimum process conditions were then irradiated using a pulsed ND:YAG laser at 300mJ, 400mJ, 500mJ, and 600mJ. The effects of the laser treatments were investigated through optical microscopy, scanning electron microscopy, energy dispersive X-ray spectroscopy, X-ray diffraction spectroscopy, and microhardness testing. The results revealed that whereas laser irradiation at 500mJ enhanced the surface properties of the shape-memory alloy, laser irradiation at 650 mJ damaged the surface of the alloy.*

**Keywords:** Shape Memory Alloys, Powder Metallurgy, SEM, NiTi.

### 1. INTRODUCTION

Shape-memory alloys have extensive numerous applications in arrange of technological fields given their excellent properties. The shape-memory i.e., the recovery of a “memorized” shape after deformation, is attributed to thermo-elastic martensitic transformation. For example NiTi shape-memory alloy has potential novel biomedical applications given its super-elasticity, shape-memory properties, and biocompatibility [1]. Nitinol is the most common type of shape-memory alloy. It is based on Ni and Ti, the most popularly used metals in shape-memory alloys with commercial applications [2]. Shape-memory alloys are subjected to various surface-treatment techniques and protocols for improving their corrosion resistance and increasing their available bioactive surfaces. These methods include mechanical and electrochemical treatments, chemical etching, heat treatments, conventional and plasma-ion immersion–implantation, laser and electron-beam irradiation [3]. Laser-based surface modification techniques are the most commonly used surface-engineering tools because they enable rapid heating and melting that subsequently extend the solid solution, refine microstructures, and homogenize alloy composition to yield products with excellent metallurgical interfaces [4]. Laser surface treatment is a highly effective means for modifying the surface properties of materials [5] because of its flexibility, high precision, and intense beam power [6]. The electromagnetic radiation of a laser beam is absorbed within the surface layer of metals. Thus, laser energy can be deposited at the exact point where it is needed. The bulk properties of NiTi

---

\* Corresponding Author: [kadkinani@gmail.com](mailto:kadkinani@gmail.com)

alloy are unaffected by laser surface treatment [7]. Furthermore, several studies such as Sadrnezhad, *et al.* (2004) [8] reported that commercially pure nickel-titanium powders were compacted and sintered at different temperatures for different times. Amorphization and interatomic phase formation were determined by X-ray diffractometry, scanning electron microscopy and differential scanning calorimetry. Porosity, virtual density B. V. Krishna (2007) [9] investigated the influence of laser parameters on the microstructure, mechanical properties, and phase conversion performance of NiTi alloys formed via laser engineered net shaping (LENS). Ni<sub>55.2</sub>-Ti<sub>44.8</sub> was fabricated using a conventional technique and formed into a cylindrical shape to achieve microstructural and mechanical properties. A. Shelyakov (2015) [10] investigated the effect of pulsed Excimer laser radiation (wavelength 248 nm at pulse width 20 ns) on the structure of Ni-Ti-Cu alloy. An Ni<sub>25</sub>-Ti<sub>50</sub>-Cu<sub>25</sub> alloy was prepared using the melt spinning method. The sample was subjected to a furnace at a temperature of 500 °C for 300 s to obtain SME. The number of pulses was changed from 1 to 100 at a repetition rate of 20 Hz with an energy density of 17 mJ/mm<sup>2</sup>.

Scanning electron microscope and X-ray investigations were performed to obtain results and determine that the thickness of the modified layer increased with increasing number of pulses and led to the creation of a structural formless crystalline compound, which evidently indicated a two-way SMA.

This work aims to study the effect of different laser energies on the structural and physical properties of the Ni-Ti-Cu shape memory alloy.

## 2. EXPERIMENTAL WORK

### 2.1 Materials

Samples of Ni-Ti-Cu shape-memory alloys were prepared through the powder metallurgy method. First, 50% titanium powder was combined with 46% nickel and 4% copper powders by weight with high purity (>99%). The powders were mixed using an electrical mixer at a rotational speed of 70 rpm for two hours in accordance with reference [11].

### 2.2 Sample Preparation

The powder mixture was compacted using a single-action tool steel mold in a press machine under 600, 700, and 800 MPa into cylinders 11 mm in diameter and 16.5 mm in length. Table 1 shows the alloy composition, compacting pressure, and sintering temperature used in this experiment.

**Table 1** Composition and Dimensions of samples with compacting pressure and sintering temperature

Alloy composition (%)	Ti <sub>50</sub>	Ni <sub>46</sub>	Cu <sub>4</sub>
Compacting pressure (MPa)	600	700	800
Sintering temperature (°C)	850	900	950
Samples dimensions(mm)	11 mmdiameter and 16.5mm length		

The compaction displacement rate of the press machine was 1 mm/min. The holding time of the machine was set at 4 minutes to ensure that the desired sample dimensions were achieved. The samples had sufficient green strength for handling after compaction. Green samples were sintered in an electric vacuum tube furnace at 850 °C, 900 °C, and 950 °C for 5 hours. The shape memory effect test was conducted by compressing the samples by 0.06% of their original lengths at a displacement rate of 1 mm/min and then heating at 110 °C for 5 minutes. The compressed samples were then allowed to slowly cool in the open air. SME (shape memory effect %) was calculated by applying the following equation:

$$\text{Shape Effect \%} = \frac{L_2 - L_1}{L_0 - L_1} \times 100 \quad (1)$$

Where:

$L_0$ : original sample length

$L_1$ : sample length after compaction by 0.06%

$L_2$ : recovered length after heating.

Shape memory effect was optimized using the Minitab program, specifically the design of experiment (DOE) tool and regression analysis. The DOE was used to investigate the effect of input variables on an output response. Regression analysis was conducted to identify the optimum SME. After obtaining the conditions (compacting pressure and sintering temperature) that give the optimum SME the sample was manufactured using the powder metallurgy method. Then, the optimized samples were then irradiated by a pulsed Nd: YAG laser. The surface temperature of the sample must not exceed 300 °C in order to avoid thermal damage [13]. Thus, the following equation was used to determine the laser energy that exerts the optimum surface effect without causing thermal damage:

$$T(Z, t) = \frac{2H}{K} \left[ \sqrt{kt} \operatorname{ierfc} \left( \frac{Z}{2\sqrt{kt}} \right) \right] \quad (2)$$

$$\operatorname{ierfc}(0) = \frac{1}{\sqrt{\pi}} \quad (3)$$

In this equation,

T: Surface temperature

Z: Depth (This parameter has a value of 0 in this experiment because only the sample surface was irradiated)

t: Time (300 ms)

H: Surface power density

K: Thermal conductivity (0.1 w/cm)

k: Thermal diffusivity ( K/ρC m<sup>2</sup> /s)

C: Specific heat capacity (322 J/kg)

ρ: Material density (6.5 g/cm<sup>3</sup>)

The laser irradiation parameters used in this study are listed in Table (2).

**Table 2** Parameters of Nd: YAG laser

Laser parameters	Characterizations
Laser energy	300,400,500,600 mJ
Time	300ms
Spot size	11mm
Number of pulses	6
Wavelength	1064nm

The microstructures of the samples were inspected using optical microscopy under 10× magnification and scanning electron microscopy (SEM) under vacuum atmosphere (1000× at 100 μm) to determine the effect of different laser energy pulses on the microstructure of the alloys. X-ray diffraction spectrometry (XRD) was performed to analyze the different phases present in the optimized samples. Sample hardness was measured using a digital microhardness tester.

### 3. RESULTS AND DISCUSSION

#### 3.1 Shape-Memory Effect Test Result (SME):

Shape memory effect percent was measured under different compacting pressure and sintering temperatures. From Figure 1, it is clear that the shape memory effect increased by increasing of compacting pressure due to the elimination of porosity, the pore number decrease and it becomes more uniform. The maximum shape recovery was 83.4% at the compacting pressure of 800 MPa and sintering temperature of 850 °C. Figure 1 shows the SME% obtained under different compacting pressures and sintering temperatures.

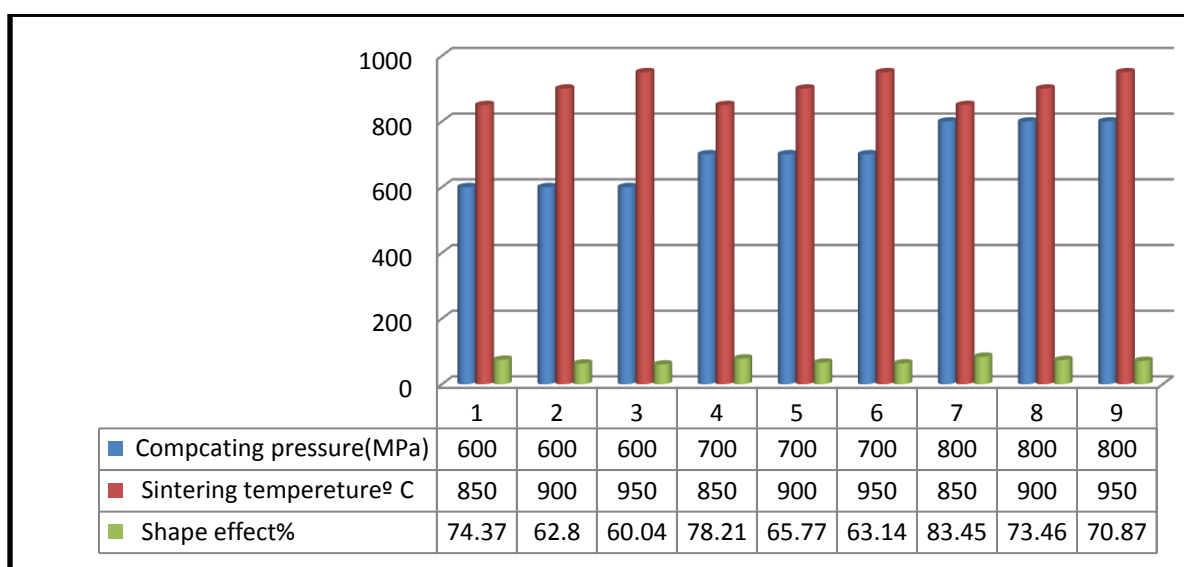


**Figure 1.** The results of shape memory effect with effect of compacting pressure and sintering temperature.

A regression equation from Minitab program was used to estimate the temperature and pressure that provide the maximum shape memory effect value. If considered the sintering temperature 750°C then the compacting pressure 882MPa was obtained Shape effect (%) = 99.98%

### 3.2 Laser Irradiation

Theoretical calculations performed using equation (2) revealed that laser energy must not exceed 672 mJ to exert the maximum surface effect on the specimens without causing thermal damage.

Experimental results showed that sample surfaces were damaged when irradiated with 650 mJ of laser energy, as shown in Figure 2. This observation validated the results of the theoretical and experimental calculations.

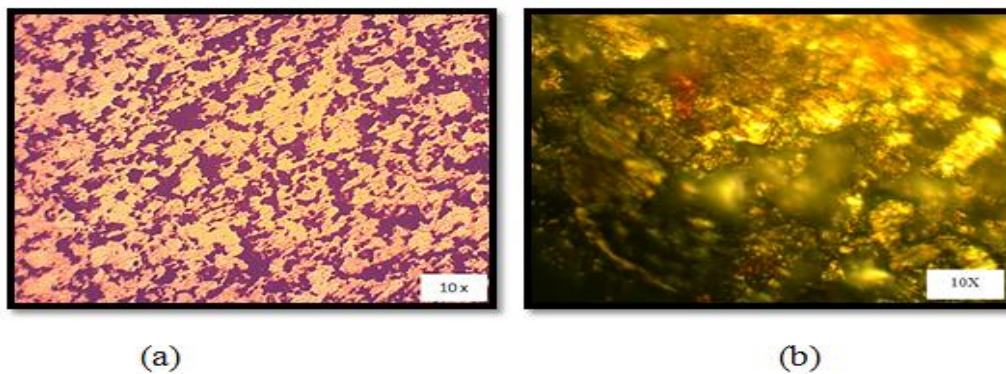


**Figure 2.** The microstructure of the surface alloy (a) before laser (b) after laser 650mJ

### 3.3 X-ray Diffraction Test (XRD)

The structural properties of Ni<sub>46</sub>-Ti<sub>50</sub>-Cu<sub>4</sub> alloy were inspected by X-Ray Diffraction analysis (XRD) before and after irradiation with different laser energies (300, 400, 500, and 600 mJ). Figures (3) to (7) show that Ni and Ti elements were converted into NiTi martensite phase (monoclinic) and austenite phase (cubic). The diffraction peak positions ( $2\theta$ ) of the as-received sample are presented at 46.3033°, 42.512°, and 43.2752°, which correspond to the 100, 201, and 111 planes, respectively.

The diffraction peak positions ( $2\theta$ ) of the sample after irradiation with a laser energy of 300 mJ are presented at 43.5413°, 51.2802°, and 39.609°, which correspond to the 111, 203, and 200 planes, respectively.

The diffraction peak positions ( $2\theta$ ) of the sample after irradiation with a laser energy of 400 mJ are presented at 42.7795°, 41.5878°, and 46.6319°, which correspond to the 012, 110, and 202 planes, respectively.

The diffraction peak positions ( $2\theta$ ) of the sample after irradiation with a laser energy of 500 mJ are presented at 44.5298°, 51.8629°, and 76.3617°, which correspond to the 111, 200, and 220 planes, respectively.

The diffraction peak positions ( $2\theta$ ) of the sample after irradiation with a laser energy of 600 mJ are presented at 44.4634°, 51.7877°, and 39.8316°, which correspond to the 100, 200, and 010 planes, respectively. In addition, the transformation of the systems that contained less than 5%

Cu is the same as that of the binary NiTi system, i.e., the austenite cubic structure is equal to the martensite monoclinic structure [15].

Tables 3 to 7 present all the XRD results, including the three strongest peak positions ( $2\theta$ ), the full width at half maximum, the experimental and standard ( $d$ ) spacing, the Miller index ( $hkl$ ), and the crystalline size variation. The crystalline size was calculated according to the Debye-Scherrer formula [16]. When the effects of different laser energies on the crystalline size of the material were compared, better CS was found with laser energy of 500 mJ, which corresponds with the results of the optical microscopy and SEM. The considerable intensities of the NiTi martensite phase and the NiTi<sub>2</sub> austenite phase are responsible for the SME of the NiTi SMAs. In addition, NiTi<sub>2</sub> precipitation is associated with the reaction of Cu with Ni and Ti atoms and with enhanced material hardness [17]. The phase Ti<sub>2</sub>(Ni<sub>1-x</sub>Cu<sub>x</sub>)<sub>3</sub> forms by solid state reaction below 850°C, Also, the laser has effect on this reaction due to increase the temperature more than phase transformation.

**Table 3** XRD result of the as received sample

$2\theta$ (deg)	FWHM (deg)	$d$ Exp (Å)	$d$ Std (Å)	$I/I_1$ %	$hkl$	C.S (nm)
46.3033	0.35160	1.9584	1.95922	100	100	24.5
42.5122	0.35000	2.1239	2.12475	66	201	24.3
43.2752	0.37700	2.0882	2.08904	52	111	22.6

From Table 3 the average value of the crystalline size was found to be equal to 23.8nm.

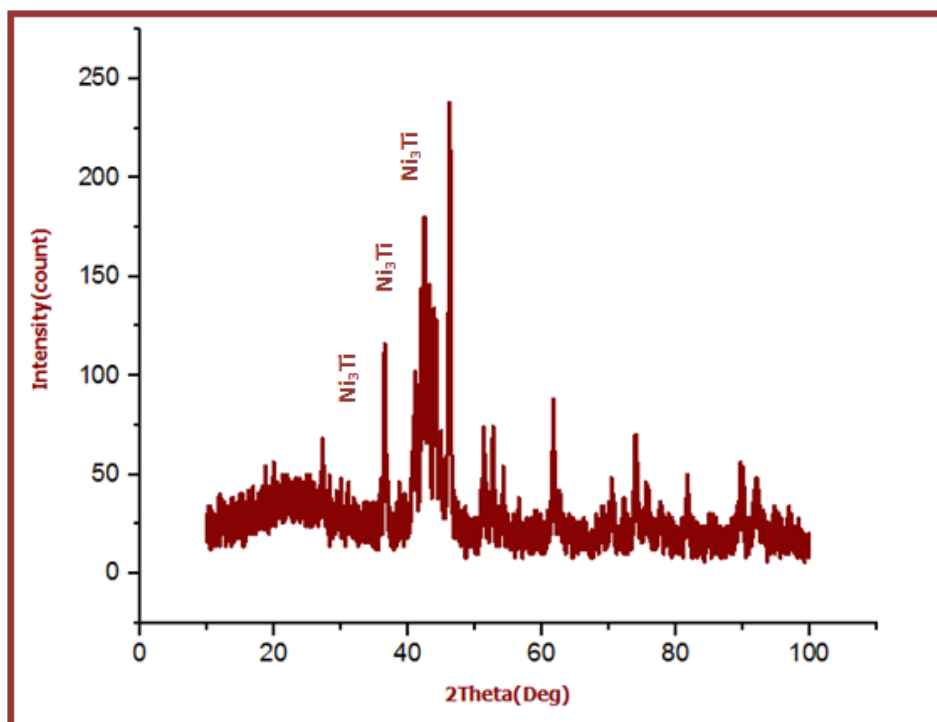


**Figure 3.** XRD test result of the as received sample.

**Table 4** XRD result of the sample after irradiated with laser energy of 300mJ

$2\theta$ (deg)	FWHM (deg)	d Exp (Å)	d Std (Å)	$I/I_1$ %	hkl	C.S (nm)
43.5413	030000	2.0760	2.05890	100	111	28.5
51.2802	0.37500	1.7794	1.78015	38	203	23.5
39.3609	0.38670	2.2863	2.28729	23	200	21.8

From Table 4 the average value of the crystalline size was found to be equal to 24.6nm.

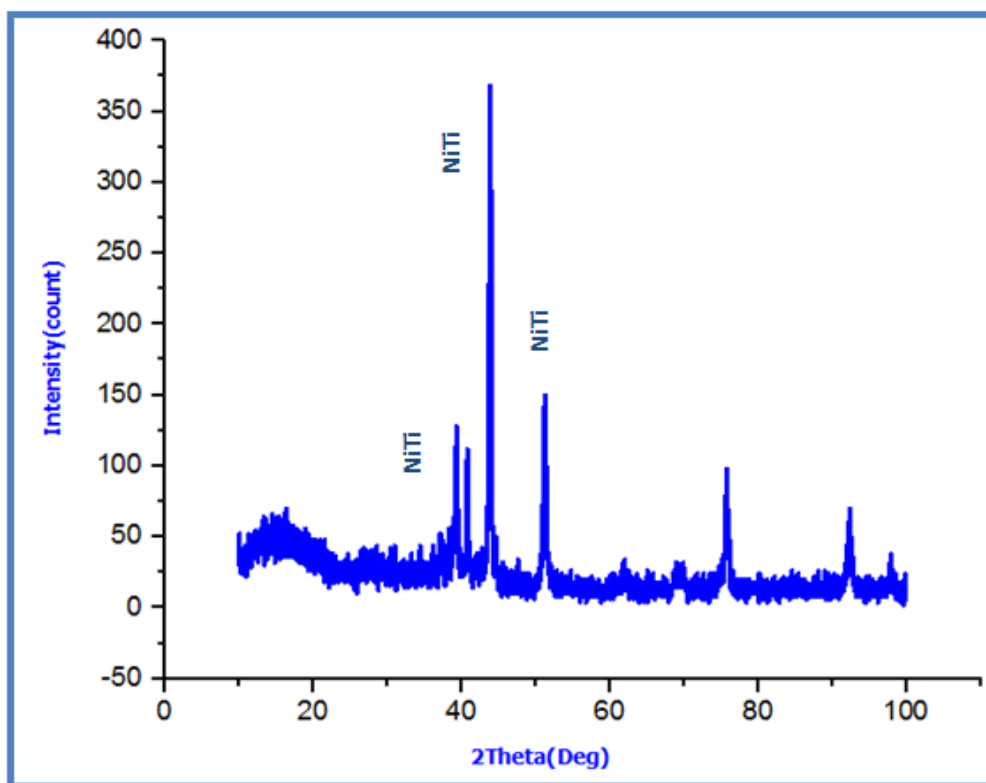


**Figure 4.** XRD result of the sample after irradiated with 300mJ of laser energy.

**Table 5** XRD result of the sample after irradiated with laser energy of 400mJ

$2\theta$ (deg)	FWHM (deg)	d Exp (Å)	d Std (Å)	$I/I_1$ %	hkl	C.S (nm)
42.7795	0.68500	2.1112	2.11209	100	012	12.5
41.5878	0.53000	2.1689	2.16981	52	110	16.0
46.6319	0.44400	1.9454	1.94618	42	202	19.5

From Table 5 the average value of the crystalline size was found to be equal to 16nm.

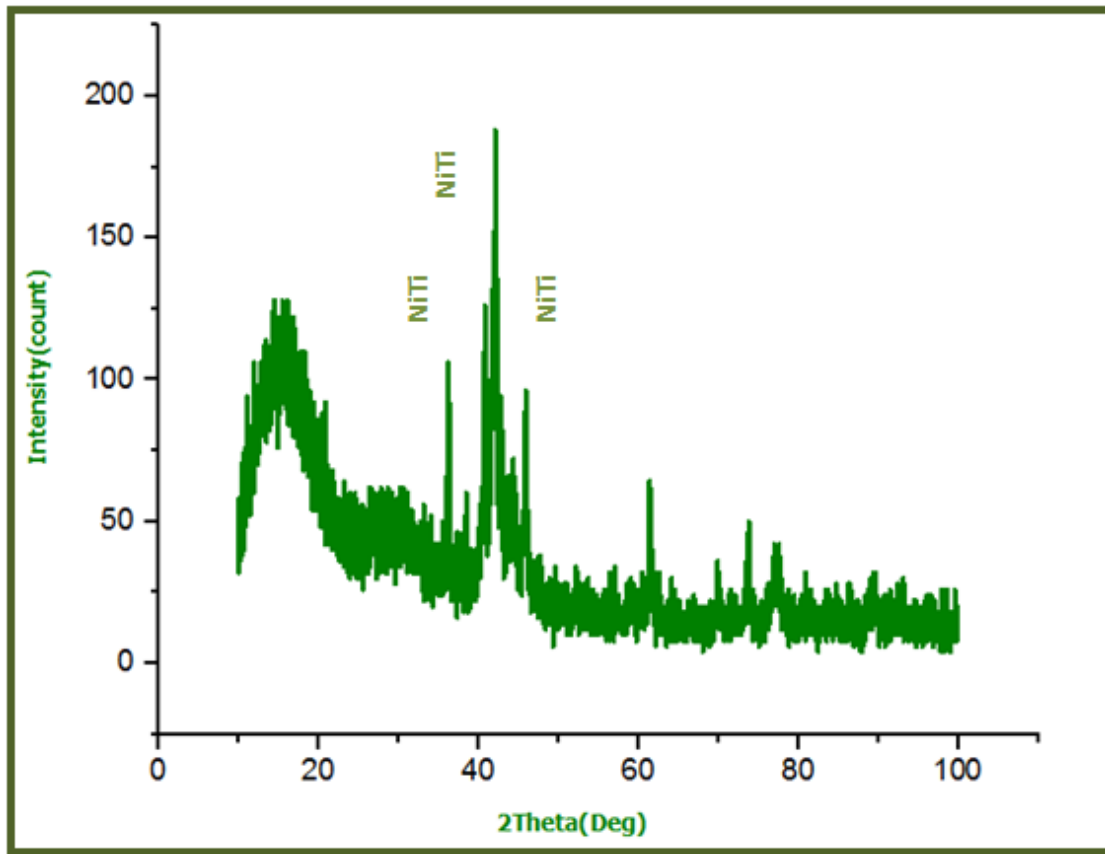


**Figure 5.** XRD result of the sample after irradiated with 400 mJ of laser energy.

**Table 6** XRD result of the sample after irradiated with laser energy of 500mJ

$2\theta$ (deg)	FWHM (deg)	d Exp (Å)	d Std (Å)	$I/I_1$ %	hkl	C.S (nm)
44.5298	0.26040	2.0322	2.03305	100	111	33
51.8629	0.28300	1.7608	1.76151	43	200	31.2
76.3617	0.28440	1.2456	1.24615	24	220	35.5

From Table 6 the average value of the crystalline size was found to be equal to 33.2nm.

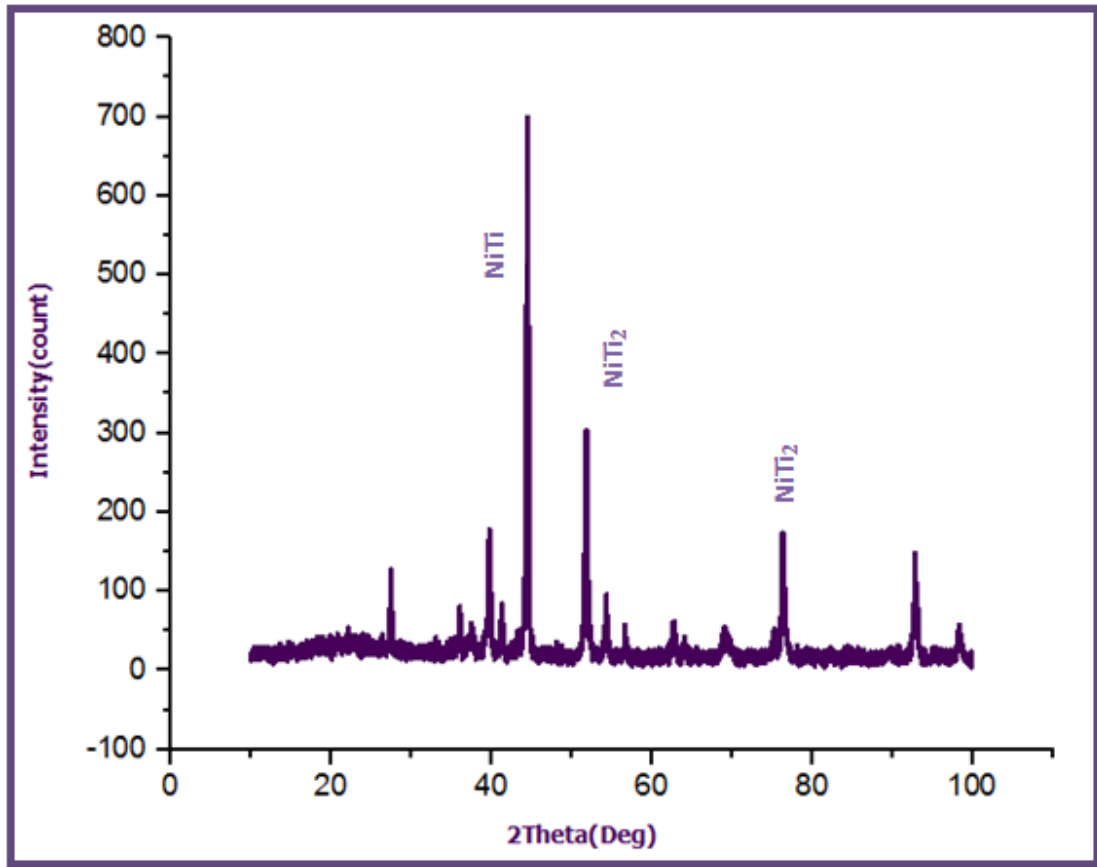


**Figure 6.** XRD result of the sample after irradiated with 500 mJ of laser energy.

**Table 7** XRD result of the sample after irradiated with laser energy of 600mJ

$2\theta$ (deg)	FWHM (deg)	d Exp (Å)	d Std (Å)	I/I <sub>1</sub> %	hkl	C.S (nm)
44.4634	0.35880	2.03513	2.03593	100	100	23.9
51.7877	0.45660	1.7632	1.76389	36	200	19.3
39.8316	0.28030	2.2604	2.26134	26	010	30.1

From Table 7 the average value of the crystalline size was found to be equal to 24.4nm.

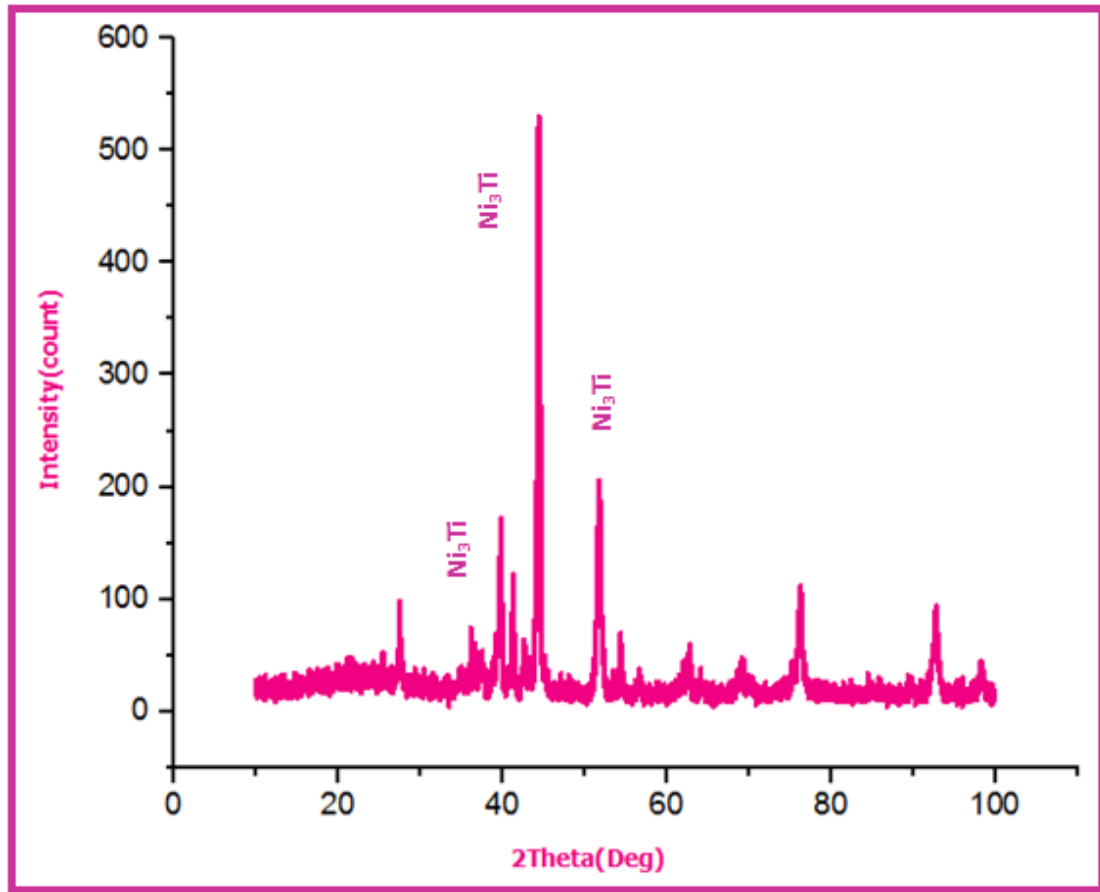


**Figure 7.** XRD result of the sample after irradiated with 600 mJ of laser energy.

#### 4. OPTICAL MICROSCOPY

The grain and grain boundary of all the tested samples appear clear in this test, thereby indicating the success of the manufacturing process.

The microstructure contains pores, as shown in Figure 8, and the percentage of these pores affects alloy density. After irradiation with different laser energies (300, 400, 500, 600 mJ), as shown in Figures 9 (a,b,c,d), the grain sizes of the samples were improved and the grain boundaries were growing because of the considerable amount of energy at the grain boundary. Irradiation with laser energy of 500 mJ [Figure (9c)] yielded the good of microstructure results because the growth of the grain boundary was increased. Figures (8) and (9) show the microstructure test results. SEM was conducted to obtained additional details.

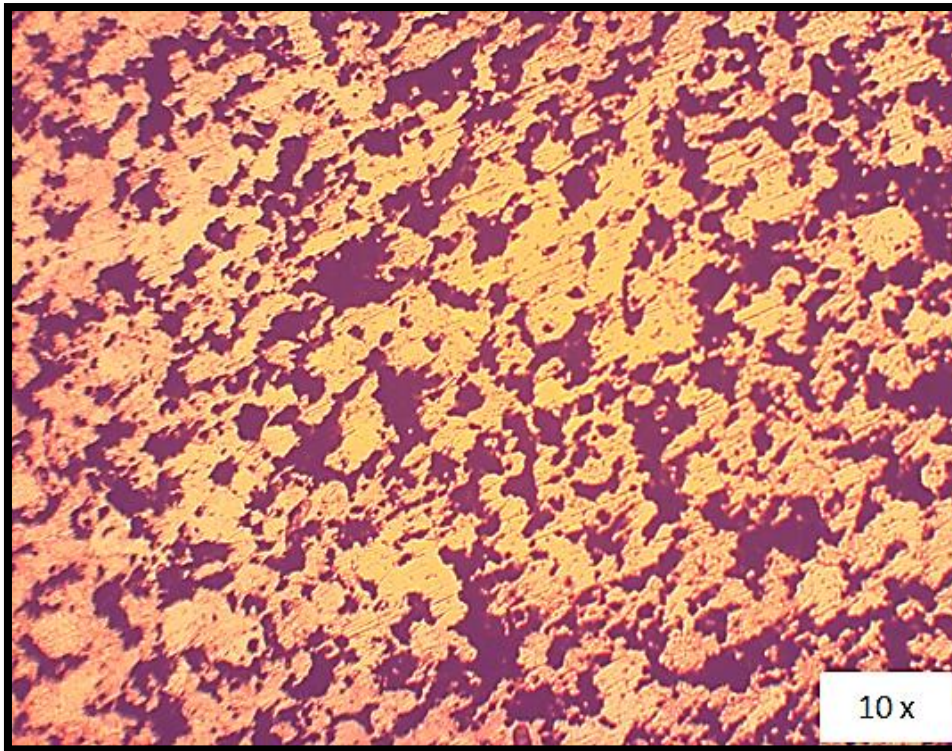


**Figure 8.** The microstructure of the as received alloy.

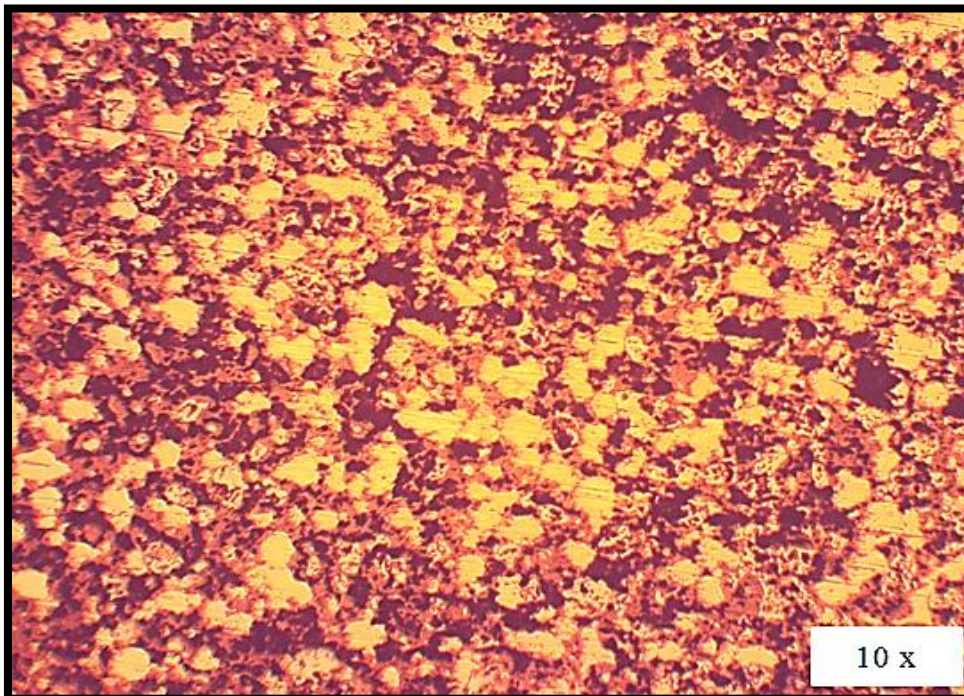


**Figure 9.** (a)

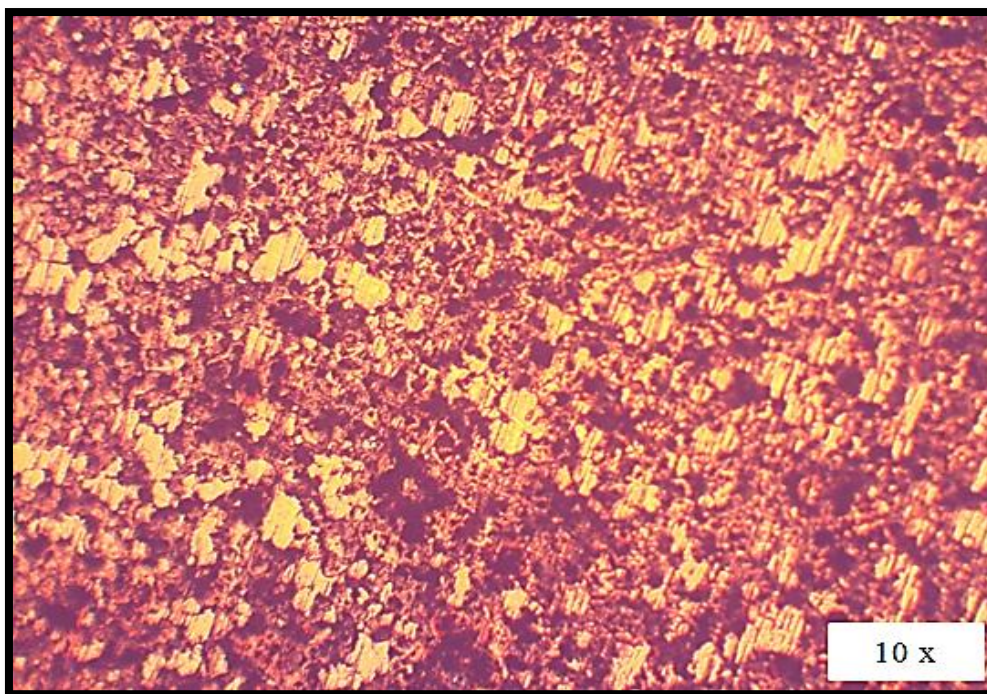


**Figure 9. (b)**

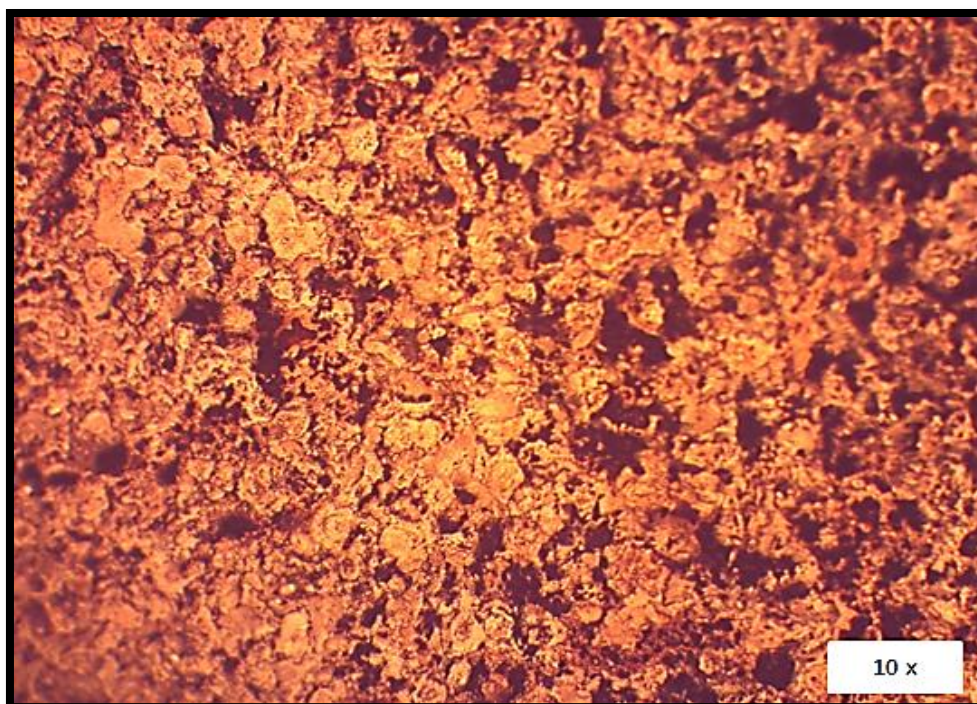


**Figure 9. (c)**

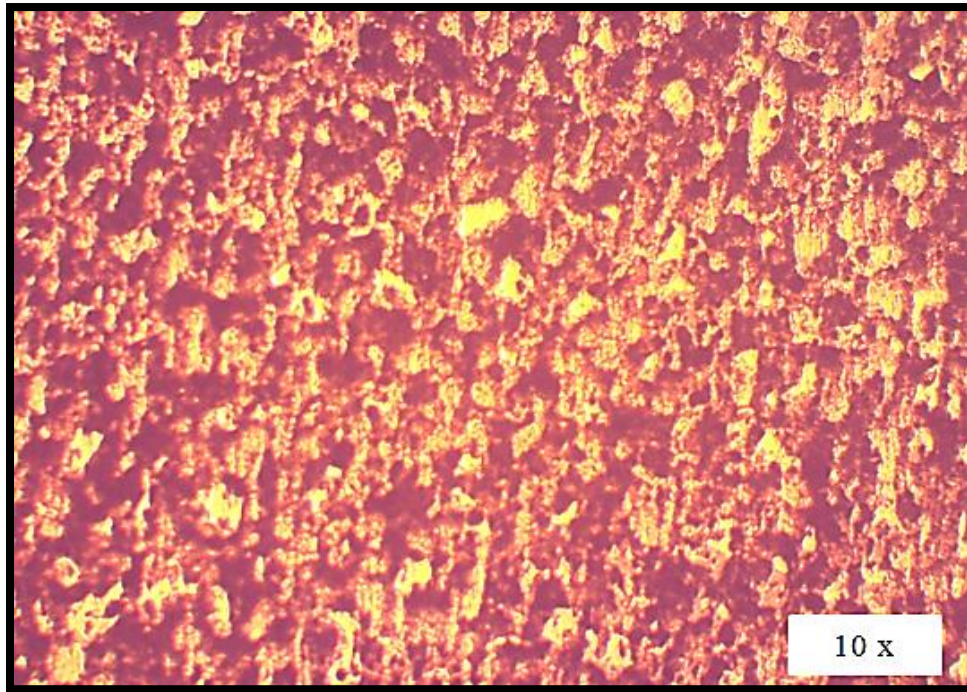


**Figure 9. (d)**

**Figure 9.** Shows the microstructure of the surface after irradiation with different laser energies (a) 300mJ (b) 400mJ (c) 500 mJ (d) 600mJ.

## 5. Scanning Electron Microscope (SEM)

Scanning Electron Microscope offers additional details about the alloy microstructure, as shown in the test image results. The samples with large grains, the formation of the grain boundary, and the appearance of pores before laser irradiation are shown in Figure (10).

The SEM images of the microstructures of the samples after irradiation with different laser energies are shown in Figures (11 a,b,c,d), which indicates that porosity decreased after laser irradiation. The irradiated region was uniform and homogeneous. These characteristics increased hardness. After comparing the different laser energies from optical microscopy and SEM, irradiation with a laser energy of 500 mJ was determined to obtain the good microstructural feature due to decrease defect.

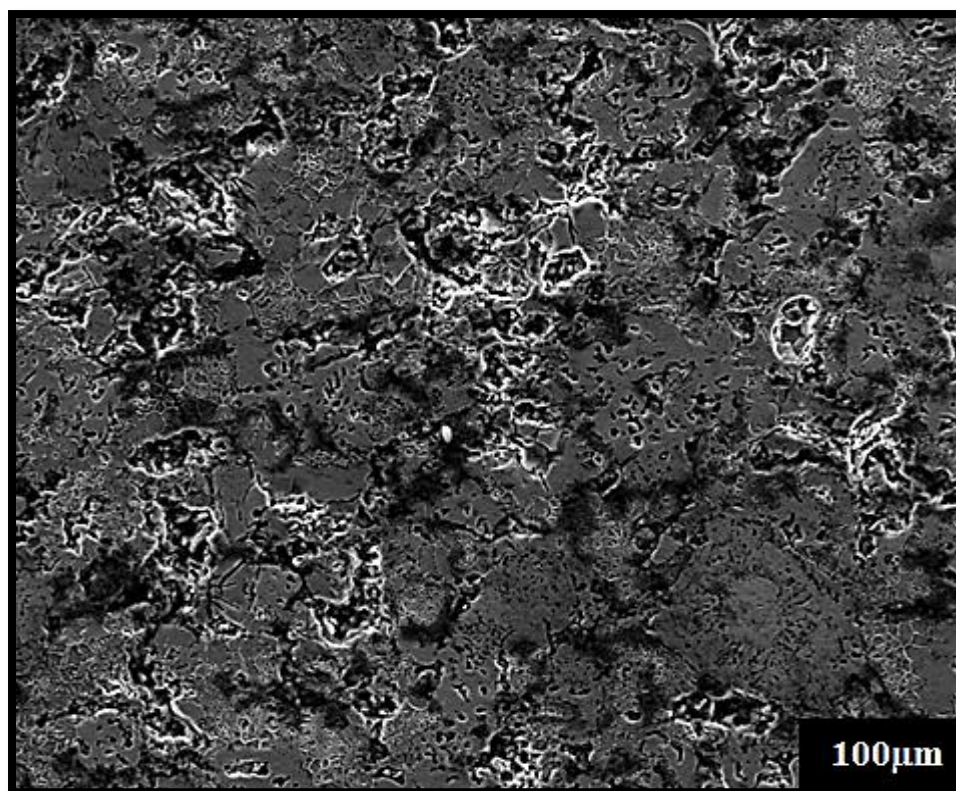


**Figure 10.** Scanning Electron Microscope of the as received sample.

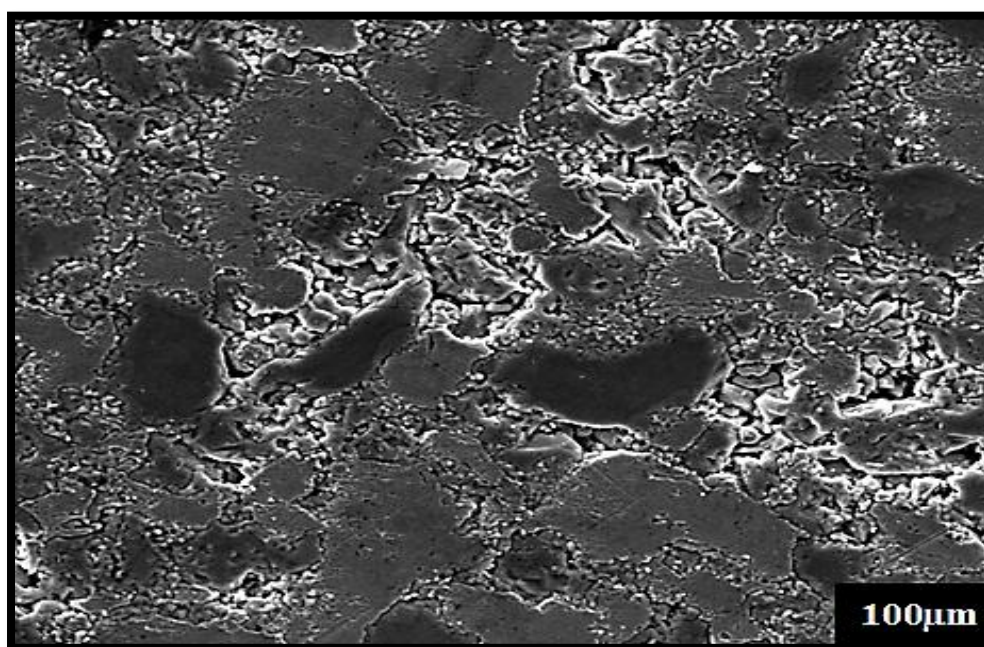


**Figure 11. (a)**

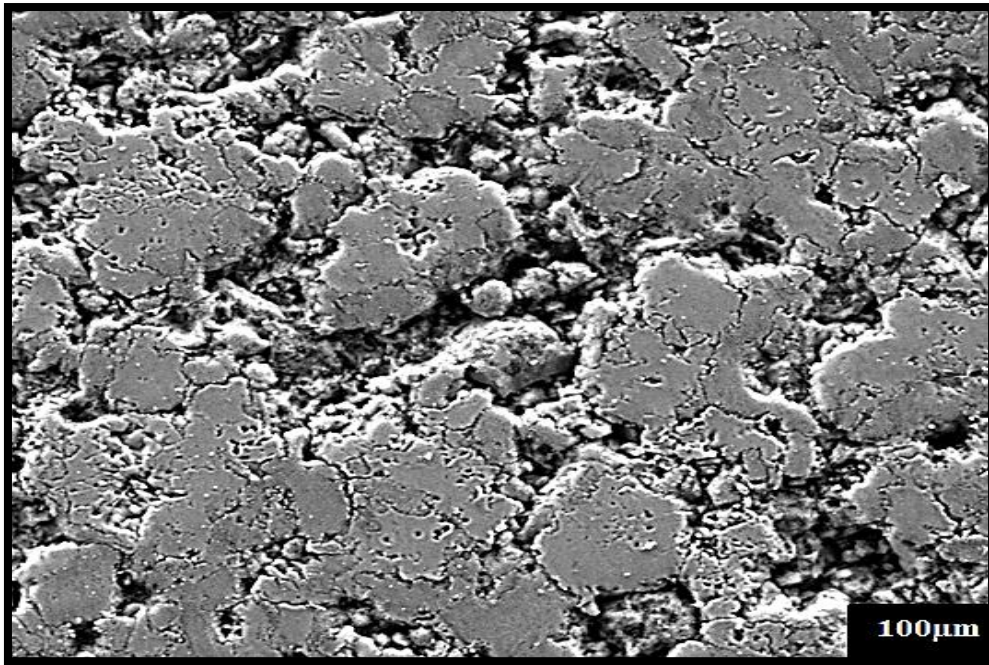


Figure 11. (b)

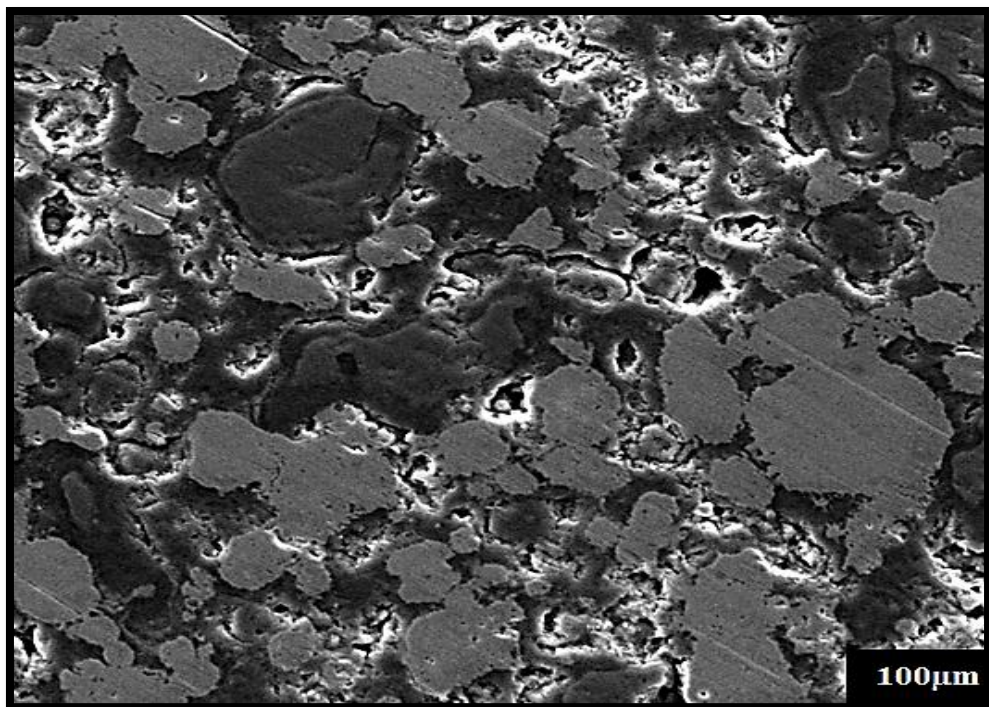
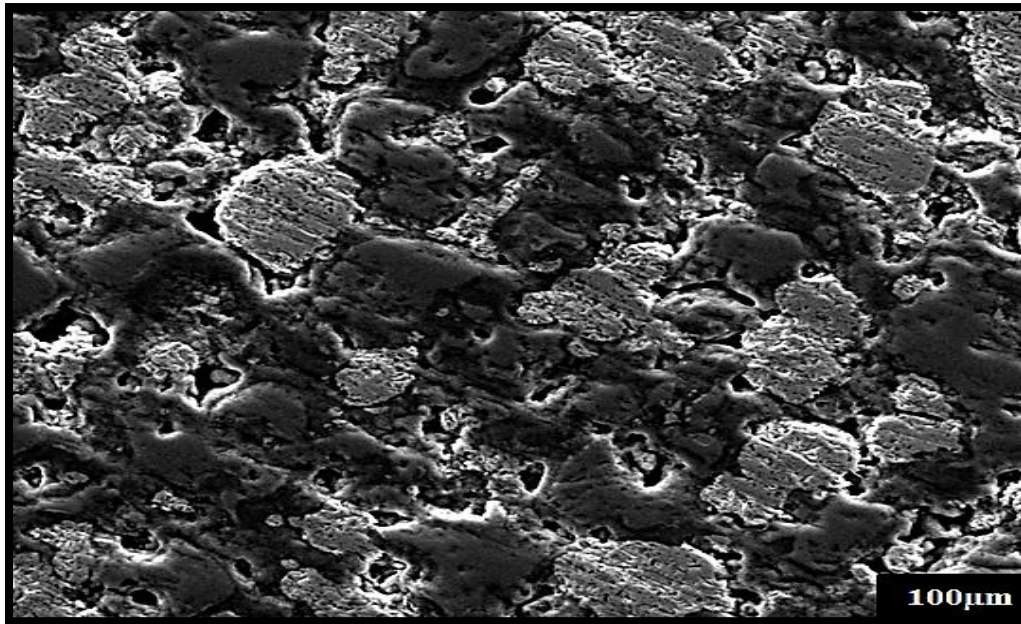


Figure 11. (c)



**Figure 11.** (d)

**Figure 11.** Scanning Electron Microscope of samples after irradiation with different laser energies (a) 300mJ (b) 400mJ (c) 500mJ (d) 600mJ.

## 6. MICROHARDNESS

The microhardness test results showed that the samples were hardened after irradiation with different laser energies (300, 400, 500, and 600 mJ). In this study, the treated surface exhibited increased hardness due to the inter-metallic compounds and grain refinement effect. The maximum increase in hardness was obtained by irradiation with 500 mJ, as shown in Figure (12). This finding corresponds to the images acquired through optical microscopy, SEM, and the XRD results.

**Table 8** Microhardness test results

Samples(Ni-Ti-Cu)	Hardness (HV)
Before irradiated with laser	204
After irradiated with different laser energies	
Energy (mJ)	Hardness (HV)
300	311
400	288.8
500	455.2
600	367.7

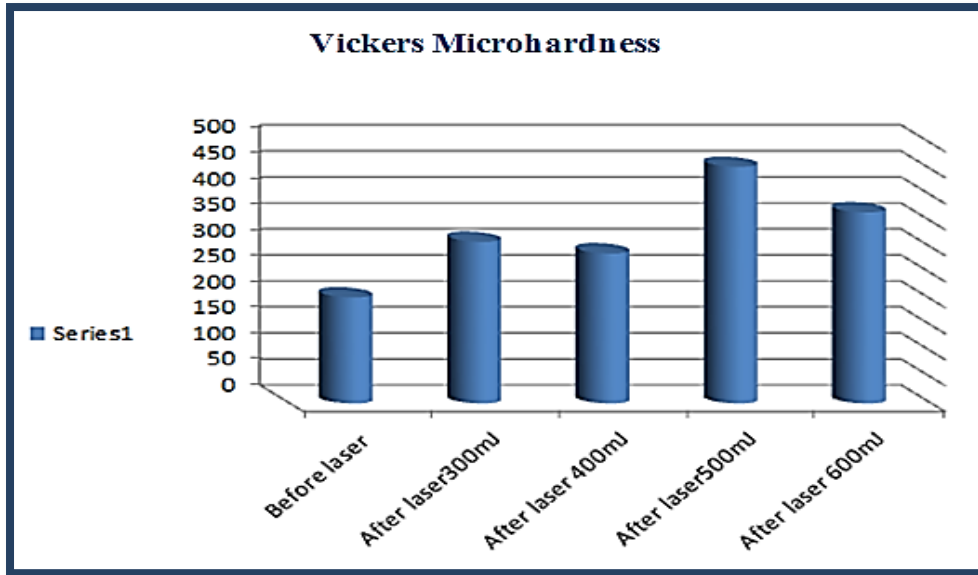


Figure 12. Hardness profile before and after irradiated samples with different laser energies.

## 7. CONCLUSIONS

- i. The results of the SME test revealed that the best recovery was 83.4% under the highest pressure of 800 MPa and sintering temperature of 850 °C.
- ii. The optimal sintering temperature and compacting pressure were identified through the Taguchi design optimization method. The optimized sample exhibited 99.98% SME recovery under 882 MPa of compacting pressure and 750 °C.
- iii. Irradiation at 500 mJ and wavelength of 1064 nm for 300 ms enhanced the structural and mechanical properties of Ni-Ti-Cu samples.

## REFERENCES

- [1] F. Villiermaux, M. Tabrizian, Y. L'H, M. Meunier & D. Piron, Excimer laser treatment of NiTi shape memory alloy biomaterials, *Applied surface science* **109**(1997) 62-66.
- [2] D. F. A. Aljuboory, K. K. Resan & A. M. Takhakh, Investigate the Microstructure and the Mechanical Properties of Ni-Ti-Cu Shape Memory Alloys, *Al-Nahrain Journal for Engineering Sciences* **20** (2017) 105-112.
- [3] S. Shabalovskaya, J. Anderegg & J. Van Humbeeck, Critical overview of Nitinol surfaces and their modifications for medical applications, *Acta Biomaterialia* **4** (2008) 447-467.
- [4] Z. Cui, H. Man, F. Cheng & T. Yue, Cavitation erosion-corrosion characteristics of laser surface modified NiTi shape memory alloy, *Surface and Coatings Technology* **162** (2003) 147-153.
- [5] Z. Cui, H. Man & X. Yang, Characterization of the laser gas nitrided surface of NiTi shape memory alloy, *Applied Surface Science* **208** (2003) 388-393.
- [6] J. Ion, *Laser processing of engineering materials: principles, procedure and industrial application*: Butterworth-Heinemann (2005).
- [7] W. M. Steen, *Laser Safety in Laser Material Processing* ed: Springer (1991) 244-252.
- [8] S. K. Sadrnezhaad & A. R. Selahi, Effect of Mechanical Alloying and Sintering on Ni-Ti Powders, *Materials and Manufacturing Processes* **19** (2004) 475-486.45.
- [9] B. V. Krishna, S. Bose, A. Bandyopadhyay, Laser Processing of Net-Shape NiTi Shape Memory Alloy *Metall. Mater. Trans. A* **38** (5) (2007) 1096-1103.

- [10] A. Shelyakov, N. Sitnikov, K. Borodako, A. Menushenkov & V. Fominski, Effect of Laser Treatment on Shape Memory Properties of TiNiCu Alloy *Phys. Procedia* **73** (2015) 108–113.
- [11] R. Hogg, Mixing and segregation in powders: Evaluation, mechanisms and processes *KONA Powder Part. J.* **27**(27) (2009) 3–17.
- [12] J. M. McNaney, V. Imbeni, Y. Jung, P. Papadopoulos & R. O. Ritchie, An experimental study of the superelastic effect in a shape-memory Nitinol alloy under biaxial loading *Mech. Mater.* **35**(10) (2003) 969–986.
- [13] S. Shabalovskaya, J. Anderegg, F. Laab, P. Thiel & G. Rondelli, Surface conditions of Nitinol wires, tubing, and as-cast alloys. The effect of chemical etching, aging in boiling water, and heat treatment, *Journal of Biomedical Materials Research Part B: Applied Biomaterials* **65** (2003) 193-203.
- [14] J. Wilson & J. Hawkes, *Lasers: Principles and Applications*, 1987 ed: Prentice-Hall, Englewood Cliffs, New Jersey.
- [15] T. Duerig & A. Pelton, Ti-Ni shape memory alloys, *Materials properties handbook: titanium alloys* (1994) 1035-1048.
- [16] P. S. Mdluli, Synthesis and Growth dynamics study of silver A thesis presented by no March (2009).
- [17] R. R. De Chimie, Phase Relations in the Niticu Shape Memory Materials **62** (2017) 539–544.